

Lyman Continuum Escape from Inhomogeneous ISM

B. Ciardi¹, S. Bianchi^{2*} and A. Ferrara³

¹ *Max-Planck-Institut für Astrophysik, Karl-Schwarzschild-Straße 1, 85748 Garching, Germany*

² *European Southern Observatory, Karl-Schwarzschild-Straße 2, 85748 Garching, Germany*

³ *Osservatorio Astrofisico di Arcetri, Largo Enrico Fermi 5, 50125 Firenze, Italy*

September 2001

ABSTRACT

We have studied the effects of gas density inhomogeneities on the escape of ionising Lyman continuum (Lyc) photons from Milky Way-type galaxies via 3D numerical simulations using the Monte Carlo radiative transfer code CRASH (Ciardi *et al.* 2001). To this aim a comparison between a smooth Gaussian distribution (GDD) and an inhomogeneous, fractal one (FDD) has been made with realistic assumptions for the ionising stellar sources based on available data in the solar neighborhood. In both cases the escape fraction f_{esc} increases with ionisation rate \dot{N}_γ (although for the FDD with a flatter slope) and they become equal at $\dot{N}_\gamma = 2 \times 10^{50} \text{ s}^{-1}$ where $f_{esc} = 0.11$. FDD allows escape fractions of the same order also at lower \dot{N}_γ , when Lyc photon escape is sharply suppressed by GDD. Values of the escape fraction as high as 0.6 can be reached (GDD) for $\dot{N}_\gamma \approx 9 \times 10^{50} \text{ s}^{-1}$, corresponding to a star formation rate (SFR) of roughly $2 M_\odot \text{ yr}^{-1}$; at this ionising luminosity the FDD is less transparent ($f_{esc} \approx 0.28$). If high redshift galaxies have gas column densities similar to local ones, are characterized by such high SFRs and by a predominantly smooth (*i.e.* turbulence free) interstellar medium, our results suggest that they should considerably contribute to - and possibly dominate - the cosmic UV background.

Key words: ISM: HII regions-radiative transfer

1 INTRODUCTION

Recent studies suggest that the ionising radiation escaping from galaxies could give a substantial (possibly dominant) contribution to the ultraviolet background radiation (UVB) during a large cosmological time span (Giallongo, Fontana & Madau 1997; Giroux & Shull 1997; Bianchi, Cristiani & Kim 2001). Also, at large redshifts, radiation from the first stellar objects has very likely driven the process of cosmic reionisation (Gnedin & Ostriker 1998; Ciardi *et al.* 2000; Miralda-Escudé, Haehnelt & Rees 2000; Gnedin 2000; Benson *et al.* 2000; Ciardi *et al.* 2001). In spite of this extensive body of work on both aspects, their predictive power is jeopardized by the persisting (theoretical and experimental) ignorance on the value of f_{esc} , the fraction of hydrogen-ionising photons that escapes from the parent galaxy into the intergalactic medium (IGM). Obviously, this quantity enters the modeling of the UVB and reionisation process and the results depend quite sensibly on the assumptions made about this poorly constrained parameter.

A promising way to make theoretical progresses on this issue is to improve the degree of realism of the modeling and the treatment of physical processes to make predictions that can be directly compared with available local and intermediate redshift data.

Dove & Shull (1994b) initially tackled the problem of determining f_{esc} by assuming smoothly varying H I distributions in the Galactic disk. They concluded that about 14% of Lyman continuum (Lyc) photons are able to escape the disk. Dove, Shull & Ferrara (2000) later improved the calculation by solving the time-dependent radiation transfer problem of stellar radiation through evolving superbubbles. Their main result is that the shells of the expanding superbubbles quickly trap ionising photons, so that most of the radiation escapes shortly after the formation of the superbubble. This results in a value of f_{esc} roughly a factor of 2 lower than obtained by Dove & Shull (1994b). Additional theoretical works (Ricotti & Shull 2000; Wood & Loeb 2000) have extended the analysis to include high-redshift galaxies, for which the escape of Lyc photons can be modified by geometrical effects (*i.e.* disk vs. spheroidal systems) and by the higher mean galactic interstellar medium (ISM) density. Generally speaking, the escape fraction decreases as the ob-

* Fellow of the European Community Research and Training Network: *The Physics of the Intergalactic Medium*.

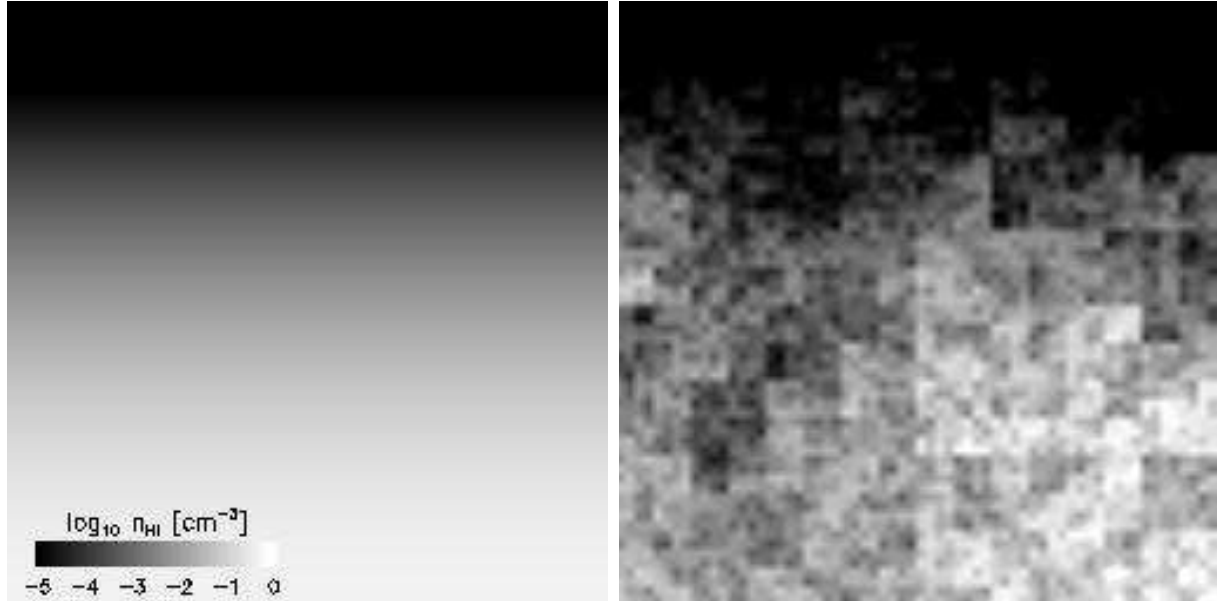


Figure 1. Slice of the Gaussian (left panel) and fractal (right panel) density distribution described in the text, cut through a plane perpendicular to the Galactic disk. The linear size is 1 kpc. Images are displayed with the same logarithmic scale.

ject virialization redshift or mass become larger; for a typical $2\text{-}\sigma$ fluctuation in a CDM model at redshift ≈ 10 these studies derive even lower values ($f_{\text{esc}} \lesssim 1\%$).

Observationally, a wide range of values for the escape fraction has been deduced, but it appears that some data favor larger values than expected from theory. For example, most of the detections of starburst galaxies with the *Hopkins Ultraviolet Telescope* and the *Far Ultraviolet Spectroscopic Explorer* (Leitherer *et al.* 1995; Hurwitz, Jelinsky & Dixon 1997; Heckman *et al.* 2001) are consistent with $f_{\text{esc}} < 10\%$, although objects have been observed with $f_{\text{esc}} < 57\%$ (Hurwitz, Jelinsky & Dixon 1997). However, absorption from undetected interstellar components could allow the true escape fractions to exceed these upper limits. Bland-Hawthorn & Maloney (1999; see Erratum 2001) used optical line emission data for the Magellanic Stream to derive $f_{\text{esc}} \approx 45\%$. Even more puzzling are the recent results (Steidel, Pettini & Adelberger 2001; Haehnelt *et al.* 2001) who detected flux beyond the Lyman limit (with significant residual flux at $\lambda < 912\text{\AA}$) in a composite spectrum of 29 LBGs at $z = 3.4$. Also, this implies that at these early epochs galaxies were much more transparent to ionising radiation than at present time, contrary to the trend found by the theoretical works mentioned before.

Can the low values of f_{esc} predicted by theory and the high values suggested by recent observations be brought into agreement? In this paper we try to ascertain if the dichotomy can be removed by considering the effects of inhomogeneities in the ISM structure and a more realistic distribution of massive stars, the primary sources of ionising photons. As already pointed out before, essentially all studies (with the partial exception of Wood & Loeb 2000) to date have derived the escape fraction assuming smoothly varying gas density distributions. However, this position is clearly untenable in the light of the large number of observations showing that the ISM in the Galaxy and nearby ones has a hierarchical, very likely fractal, structure (Elmegreen

& Falgarone 1996 and references therein). This view is also supported by theoretical works (see for example Norman & Ferrara 1996), which predict a fractal behavior over a large dynamical range. This type of organization naturally arises from turbulent pressure, which plays a crucial role in the various phases of the ISM (see for example Kulka-rni & Fich [1985] for the cold neutral HI component and Reynolds [1985] for the warm ionised medium): Norman & Ferrara (1996) showed that the ISM turbulent pressure is roughly 30 times higher than the thermal one. Turbulence is pumped into the ISM primarily by multi-SN explosions; however, reaching the high energy density of present day galaxies requires a considerable fraction of the Hubble time at high redshift. Hence the ISM of these primordial systems, differently from their local counterparts, is likely to be more quiescent and smooth.

For these reasons, it seems worthwhile to examine a model for the escape fraction in which a fractal, turbulence dominated ISM is taken into account. This is what we explore in the rest of the paper.

2 MODEL

In this section we describe the model adopted for the Milky Way (MW) gas density and the stellar distribution, as well as the source emission properties. We use the MW as a reference template, but our results should hold with good approximation for the entire class of MW-type galaxies, as long as the properties of their ISM are similar.

To study the escape of (ionising) Lyman continuum (Lyc) photons from the MW, we have chosen a representative cubic volume of 1 kpc^3 located above the disk midplane and centered at the Solar position. This allows us to exploit the high quality data available for the spatial distribution of the ionising OB stars (*e.g.* Garmany, Conti & Chiosi 1982). Also, the same argument applies to the exquisite detail with

which the gas density distribution has been derived (Dickey & Lockman 1990; Reynolds & Haffner 2001 and references therein).

Comparison between the soft X-ray background and absorption line experiments toward stars near the Sun, have suggested that we live in a rarefied, hot ISM cavity, usually known as the Local Bubble, whose average radial extent is ≈ 100 pc (Sanders et al. 1977; Snowden et al. 1990; Sfeir et al. 1999). As the volume of the Local Bubble is only 0.2% of the simulation volume, we neglect for simplicity the effects of such structure on our results.

2.1 ISM Density Distribution

In order to compare the effects of inhomogeneities on the escape of Lyc photons with previous results, we have first considered the commonly adopted Gaussian HI density distribution (GDD):

$$n_{HI}(z) = n_0 \exp(-z^2/2H^2), \quad (1)$$

where z is the height above the midplane of the disk. Such distribution is a solution of hydrostatic equation for the gas in the gravitational field of a disk galaxy, including a dark matter component. The Gaussian distribution that most closely resembles the three-component Dickey-Lockman (1990) vertical distribution has parameters $n_0 = 0.367 \text{ cm}^{-3}$ and $H = 0.184 \text{ kpc}$ (Dove, Shull & Ferrara 2000). This gives a total neutral hydrogen column density perpendicular to the disk of $N_{HI} = 5.2 \times 10^{20} \text{ cm}^{-2}$.

Observations of molecular clouds have shown that with increasing spatial resolution the gas distribution breaks up into substructures of yet smaller scales. The self-similarity of the relations linking some of the molecular cloud properties (such as the mass-size relation and the distribution functions of size and mass) suggests that the density distribution very likely has a fractal structure induced by turbulence (Falgarone, Phillips & Walker 1991; Elmegreen & Falgarone 1996; Elmegreen 1999). As a more realistic description, we have thus alternatively adopted a fractal model.

A fractal ISM distribution is obtained from hierarchically clustered points, along the prescriptions given by Elmegreen (1997). In brief, starting from a point with coordinates $(i_0, j_0) = (0.5, 0.5)$, fractals on the $x - y$ plane were made with $K = 6$ hierarchical levels by choosing continuous coordinates such that for random numbers R_i in the interval $[0,1]$, $i_1 = i_0 + 2(R_1 - 0.5)/L^1$ at the first level, $i_2 = i_1 + 2(R_2 - 0.5)/L^2$ at the second level, and so on up to level K ; $L = 2$ is a geometric factor for subdivision of one level into the next. The same procedure was used for j . At each level, $N = 5$ new positions were substituted for each position in the previous level, leaving N^K positions after K levels. At each height z , a $L^{2K} = 64^2$ square grid was placed around all the points, and the number of points inside each grid cell was counted. We thus recovered the gas density in each grid cell constraining its average value to be the same as for the Gaussian distribution of eq. 1. The resulting gas distribution has thus a fractal dimension $D = \log N / \log L = 2.32$, which is consistent with the experimentally derived value (Elmegreen & Falgarone 1996). This procedure is repeated at each of the 64 heights that have discrete values in the range $0 < z < 1 \text{ kpc}$; this range represents a good compromise between the need to encompass most of

Table 1: Simulation Parameters

Run	$n_{HI}^{(1)}$	$n_{\star}^{(2)}$	$\Sigma_{\star}^{(3)}$
A	Gaussian	Gaussian	24
B	Fractal	Gaussian	24
C	Gaussian	Gaussian	48
D	Fractal	Gaussian	48
E	Fractal	Schmidt Law	24

⁽¹⁾Density Distribution

⁽²⁾Stellar Distribution

⁽³⁾Stellar Surface Density [kpc^{-2}]

the vertical extent of the HI disk and to achieve a sufficient spatial sampling. The clumping factor of this distribution, $C \equiv \langle n^2 \rangle / \langle n \rangle^2$, calculated as a function of distance from the midplane, ranges between 4 and 8.

In principle, it would have been possible to use the HI distribution directly obtained from 21-cm line observations. However, resolving power limitations make such maps of little use to study the effects of inhomogeneities. For example, the spatial sampling of the Dwingeloo survey (Burton & Hartmann 1994) is 0.5° (corresponding to $\approx 0.03 \text{ kpc}$) but the spectral sampling is 1.03 km s^{-1} , or 0.1 kpc . This is about a factor of 6 lower than the resolution required by our simulation. Surveys with higher spatial resolution (1 arcmin) do exist, but they do not cover a sufficiently large latitude range (the best is probably the Canadian Galactic Plane Survey which covers -3.5° to $+5.5^\circ$, equivalent to half the simulation box) at roughly the same spectral resolution. Thus, we have restricted our analysis to the previous two model cases. A summary of the adopted density distributions in the various simulation runs is shown in Table 1. For illustration, in Fig. 1 we show a slice of the GDD (left panel) and the FDD (right panel) cut through a plane perpendicular to the Galactic disk.

Measurements of faint optical interstellar emission lines and pulsar dispersion measures, show that in the MW approximately 1/3 of the HI mass is contained in the Warm Ionized Medium (Reynolds 1991a; Reynolds 1993). To account for the presence of such component, we have multiplied the GDD and FDD described above by a factor of 1.3. We assume that initially the gas has a temperature of 100 K, as derived for the Cold Neutral Medium.

2.2 Stellar Distribution

Garmany, Conti & Chiosi (1982) compiled a catalog of O-type stars in the Solar neighborhood. The catalog is supposed to be complete to a distance of 2.5 kpc from the Sun. Within this radius, the surface density of such component is about $\Sigma_{\star} = 24 \text{ stars kpc}^{-2}$. Therefore, we have reproduced the local stellar population by randomly extracting positions and photon ionisation rates for 24 stars in our 1 kpc^3 computational volume as follows.

We have adopted for the stars a vertical Gaussian distribution with a scaleheight $H_{\star} = 63 \text{ pc}$, as recently derived by Maíz-Apellániz (2001) from a sample of O-B5 stars from the Hipparcos catalog. By randomly sampling this distribution, we have derived the z -coordinate of each star; the x and

y coordinates have been selected randomly. All stars above the galactic plane have been included in the simulations.

As the star formation process should preferentially take place in the densest regions of the ISM, we have also produced stellar distributions assuming that the probability of finding a star in a certain region is proportional to a power of the gas density, $P \propto \rho^{1.5}$, *i.e.* a Schmidt-type law (Kennicutt 1998).

Finally, we have also produced stellar distributions with a surface density two times larger than the local one, $\Sigma_* = 48 \text{ kpc}^{-2}$, to study the dependence of f_{esc} on a larger range of ionisation rates. A summary of the adopted stellar distributions is shown in Table 1.

2.3 Source Emission Properties

A spectral type and luminosity class has been randomly assigned to each star, using the number frequencies of objects of a given type in the catalog of Garmany, Conti & Chiosi (1982). Within 2.5 kpc from the Sun, about 50% of the stars are of O9.0 - O9.5 types, half of which of luminosity class V. We have then used the stellar models of Schaerer & de Koter (1997) to derive the rate of ionising photons from the given spectral type and luminosity class.

Following this recipe, we have produced 20 different stellar distribution realizations for each case in Table 1, to get some semblance of the scatter among different realizations. The scatter is produced by the random sampling of the number, position and ionising photon rate of individual stars in the simulation volume.

For simplicity, we have adopted a single black-body spectrum for each star. We have assumed a temperature of 40000 K, a mean value for the effective temperatures of O-type stars ($T_{eff} = 30000 - 50000 \text{ K}$; Schaerer & de Koter, 1997). The pattern of ionisation does not heavily depend on the detailed shape of the spectrum, as long as most of the ionising photons are emitted close to the HI ionisation limit.

Early B-type stars also produce ionising radiation. Assuming a Salpeter Initial Mass Function (IMF) and the ionising photon rate of Schaerer & de Koter (1997), we have estimated that B0-B0.5 stars contribute on average to less than 10% of the total number of ionising photons. We have run a few simulations to check the influence of B stars. The difference between models with and without B stars are masked by the random scatter in the results. Therefore, we did not include B-type stars in the stellar distributions.

3 RADIATIVE TRANSFER SIMULATIONS

To study the propagation of ionising radiation produced by the stars through the given ISM density distribution we use the Monte Carlo (MC) radiative transfer code **CRASH** (*Cosmological RAdiative transfer Scheme for Hydrodynamics*), described in Ciardi *et al.* (2001). The code has been originally developed for cosmological applications, but below we show that it can correctly handle also the rather different conditions prevailing in the interstellar medium of galaxies. For clarity, we briefly summarize the main features of the numerical scheme relevant to the present study.

In the application of a MC scheme to radiative transfer

problems, the radiation intensity is discretized into a representative number of monochromatic photon packets. The processes involved (e.g. packet emission and absorption) are then treated statistically by randomly sampling the appropriate distribution function. The 1 kpc^3 simulation volume has been discretized in 64^3 grid cells; we consider absorption by HI and dust; we neglect the contribution of He because of the paucity of the He-ionising photons produced. We have estimated the dust optical depth in the optical using the canonical relation between the HI column density, N_{HI} , and the color excess $E(B-V)$ (Bohlin, Savage & Drake 1978). This has been converted into an optical depth at the ionisation limit by adopting the far-UV parametrization of the mean Galactic extinction law (Fitzpatrick & Massa 1988). We obtain:

$$\tau_d(912\text{\AA}) = 1.9 \times 10^{-21} (N_{HI}/\text{cm}^{-2}), \quad (2)$$

where we have excluded the contribution of dust scattering to the opacity, by multiplying for $(1 - \omega)$; $\omega = 0.4$ is the average albedo of dust in the UV close to the ionisation limit (Witt *et al.* 1993). Given the above equation, as the final mean ionisation fraction for run A (run B) is $\langle x \rangle = 0.69$ (0.40) (see Section 4), for the frequencies of interest here, we find that $\tau_d/\tau_{HI} < 2.46 \times 10^{-2}$ (1.28×10^{-2}). Thus, dust contribution to absorption is negligible.

For the range of densities considered here, a number of photon packets equal to $\mathcal{N}_p = 5 \times 10^7$ has to be emitted in order to reach numerical convergence.

Differently from Ciardi *et al.* (2001), here we deal with more than one ionising source. We have found that, if the number of emitted packets is sufficiently high, a more reliable solution of the discretized time-dependent ionisation equation is obtained if the time step Δt used in their eq. 10 is not treated statistically. Thus, here Δt is the time elapsed since a photon packet has gone through the cell for which the equation is being solved. Only photons escaping from the top side of the cubic region contribute to the escape fraction, while those escaping from side faces or the bottom one are subject to a reflecting boundary condition, thus simulating photons coming from adjacent regions.

The same numerical tests of the code described in Ciardi *et al.* (2001) have been performed in an interstellar (rather than intergalactic) environment. We do not report them here; instead, in Fig. 2 we show the evolution of ionised regions (in black) produced in the GDD described in the previous Section, by sources with different ionisation rate, located on the disk midplane. The slices show a plane perpendicular to the Galactic disk through each source location. Different columns refer to different source ionisation rates ($\dot{N}_\gamma = 1.8, 16, 34 \times 10^{48} \text{ s}^{-1}$ respectively, from left to right), while from the top to the bottom we show the ISM ionisation structure at times $t = 0.05, 1, 1.5, 5 \text{ Myr}$ after the source has been turned on. The solid lines correspond to the stationary analytical solution given in Dove & Shull (1994b). The ionisation rates were chosen in order to reproduce the various possible shapes of the ionised regions: spherical, elongated and funnel-like.

To prevent misunderstandings, it is useful here to give our working definition of the escape fraction. We define the *global* escape fraction, $f_{esc,g}$, as:

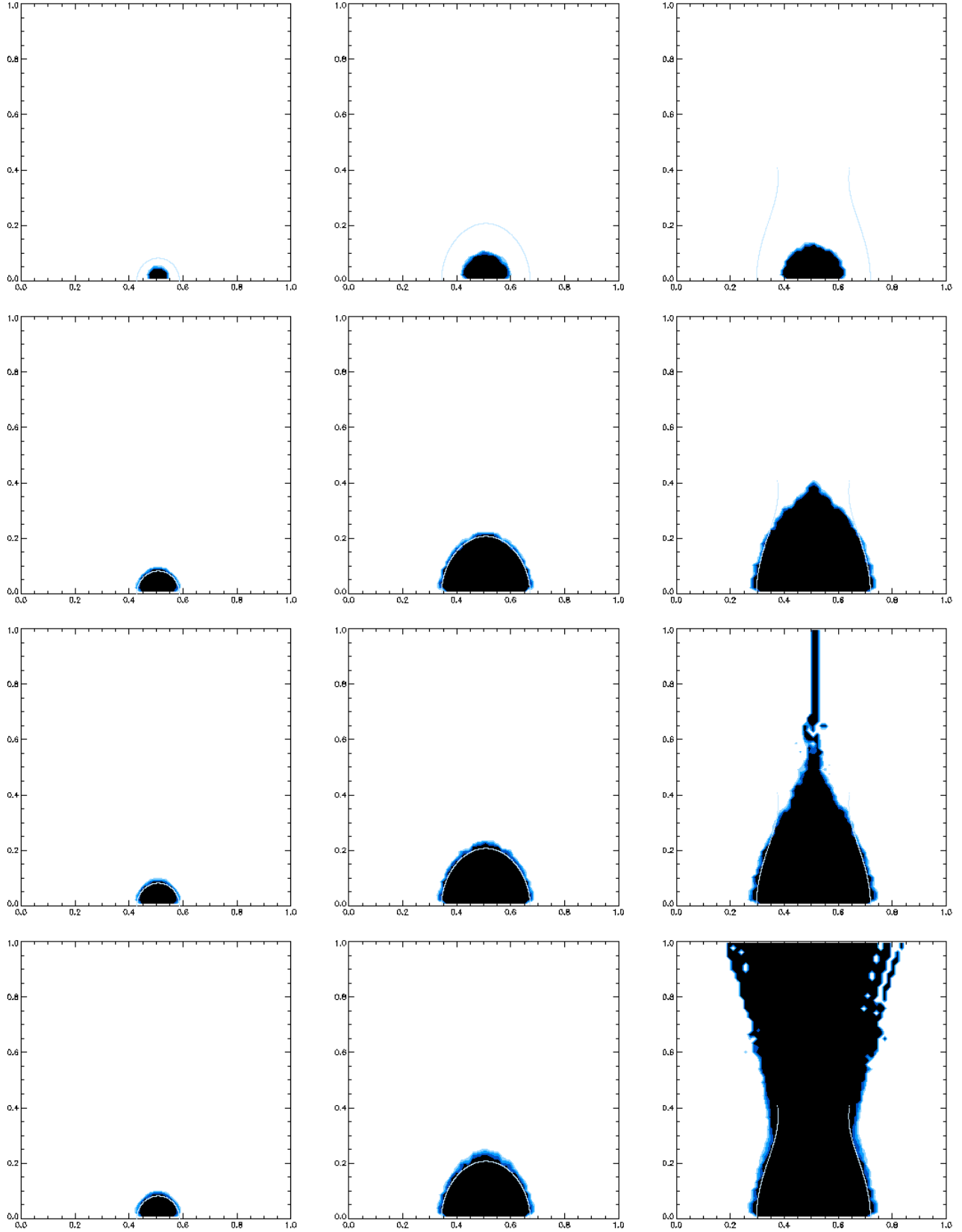


Figure 2. Evolution of ionised regions (black) produced in the GDD described in Section 2, by sources with different ionisation rate, located on the midplane of the disk. The linear box size is 1 kpc. Columns, from the left to the right, refer to a source ionisation rate of $\dot{N}_\gamma = (1.8, 16, 34) \times 10^{48} \text{ s}^{-1}$ respectively; from the top to the bottom the ionisation structure at a time $t = (0.05, 1, 1.5, 5) \text{ Myr}$ after source turn on is shown. The solid lines correspond to the stationary analytical solution (Dove & Shull 1994b).

$$f_{esc,g}(t) \equiv \frac{\int_0^t dt \dot{N}_\gamma^e(t)}{\int_0^t dt \dot{N}_\gamma(t)}, \quad (3)$$

where \dot{N}_γ^e is the escaping photon rate (*i.e.* the number of photons reaching $z \geq 1$ kpc per unit time) and \dot{N}_γ is the total photon rate production at (simulation) time t . The *instantaneous* escape fraction, $f_{esc,i}$, is instead given by:

$$f_{esc,i}(t) \equiv \frac{\dot{N}_\gamma^e(t)}{\dot{N}_\gamma(t)}. \quad (4)$$

In order to derive f_{esc} , we assume that the stars have a constant ionisation rate and we run the simulation until convergence (*i.e.* the escape fraction and the ionisation structure do not change) is reached. As we find that, after a time of $\sim 5 \times 10^6$ yr the value of f_{esc} remains roughly constant, we stop the simulations after $\sim 10^7$ yr. This is expected as the recombination time at the midplane is 0.3 Myr.

Following the method described above, we have run 20 simulations for each of the cases indicated in Table 1.

4 RESULTS

In Fig. 3 we show the evolution of the global escape fraction, $f_{esc,g}$, as a function of the total ionisation rate, \dot{N}_γ , for runs A (filled triangles in Fig. 3a) and B (filled circles in Fig. 3b). In both cases $f_{esc,g}$ increases with increasing \dot{N}_γ , although for the FDD with a flatter slope. The reason for this different behavior is that photons in a GDD can escape only if an ionised channel can be produced by the stars themselves. Consequently, a low ionisation rate results in a low escape fraction. In a FDD instead, photons can travel along clear sightlines through low density ionised channels and escape more easily. Thus, for $\dot{N}_\gamma \lesssim 2 \times 10^{50} \text{ s}^{-1}$ $f_{esc,g}$ is always higher for a FDD, while for larger ionisation rates a GDD becomes more transparent. In both cases, the scatter in $f_{esc,g}$ is mainly due to differences in the star position and ionisation rate.

To study the effect of a larger total ionisation rate, we have increased the stellar surface density, as explained in Section 2, obtaining a maximum value $\dot{N}_\gamma \simeq 5 \times 10^{50} \text{ s}^{-1}$. These additional runs are represented in Fig. 3 as open triangles (run C) and circles (run D). The scatter is reduced with respect to runs A and B as, increasing the number of stars, their position affects less sensibly the value of f_{esc} , which instead depends more strongly on the total ionisation rate. In order to check if the curve for the GDD would reach a plateau or rather keep growing (as the analytical derivation by Dove & Shull 1994a suggests), we have increased the total ionisation rate up to a value of $\simeq 8 \times 10^{50} \text{ s}^{-1}$ (corresponding to a stellar surface density of $\Sigma_\star \simeq 120 \text{ kpc}^{-2}$). As we expect the scatter to be reduced, in order to limit the computational time, we have only run 6 different realizations.

The evolution of $f_{esc,g}$ is linear over the considered range of \dot{N}_γ and it can be fitted by the following function:

$$f_{esc,g} = \alpha(\dot{N}_\gamma/10^{50} \text{ s}^{-1}) + \beta, \quad (5)$$

where for a GDD (FDD) $\alpha = 0.089 \pm 0.003$ (0.023 ± 0.003) and $\beta = -0.07 \pm 0.01$ (0.07 ± 0.01). In both cases the fit is represented as a dotted line in Fig. 3. We find that the GDD

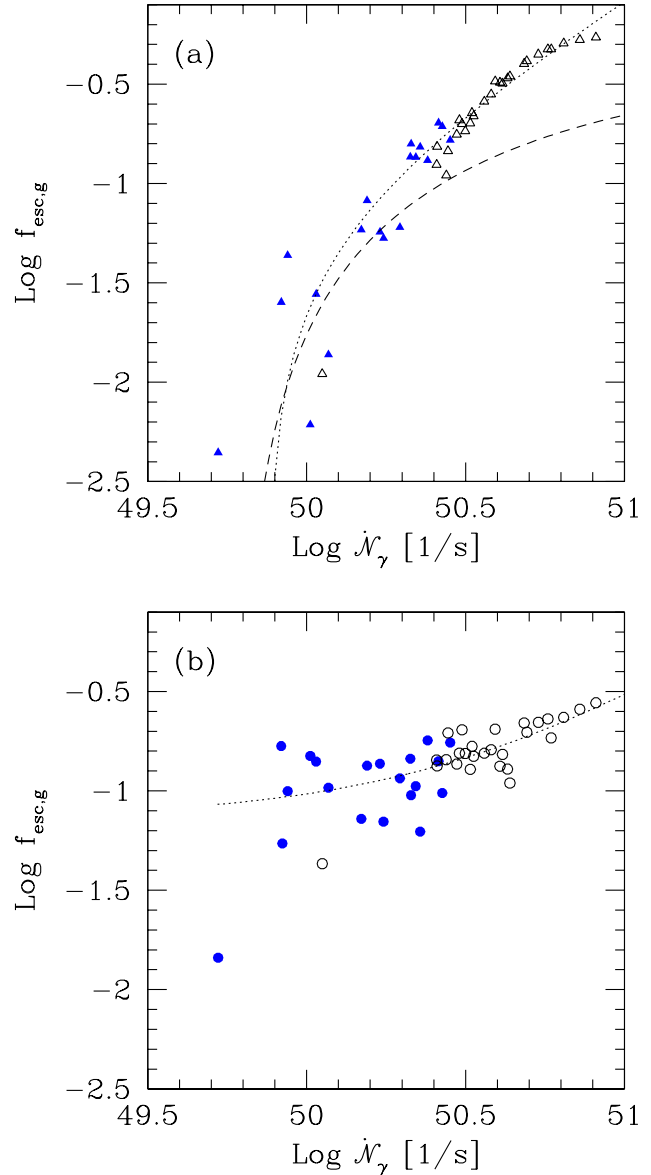


Figure 3. (a) Evolution of the global escape fraction, $f_{esc,g}$, as a function of the total ionisation rate, \dot{N}_γ , for runs A (filled triangles) and C (open triangles). The dotted line is the fit given by eq. 5. The dashed line is the analytical solution derived by Dove & Shull (1994a), assuming a single source located on the galactic plane. (b) Same as (a) for runs B (filled circles) and D (open circles).

curve eventually flattens and departs from the fit in eq. 5; on the contrary the results for the FDD are well described by the same fit also for high values of \dot{N}_γ .

Dove & Shull (1994a) derived analytically the value of f_{esc} expected in a GDD from a point source of given ionisation rate, located on the disk of the Galaxy. The value they obtained (represented by a dashed line in Fig. 3a) should be compared with the asymptotic value of $f_{esc,i}$. However, as for late evolutionary times $f_{esc,g}$ approaches $f_{esc,i}$ (see below), we can compare their results with our runs A and C directly from Fig. 3a. Clearly, the evolution of $f_{esc,g}$ differs from the analytic calculation and higher values for the escape fraction are obtained, especially for large ionisation

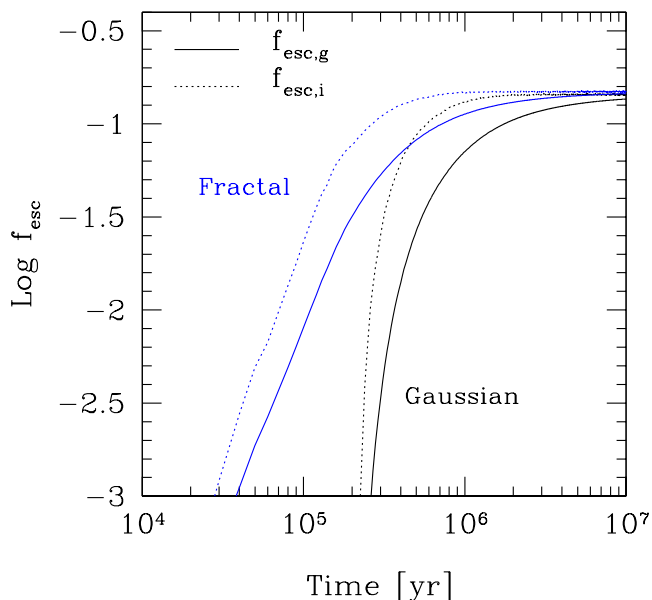


Figure 4. Time evolution of the escape fraction for a Gaussian (lower curves) and a fractal (upper curves) density distribution. The evolution of $f_{esc,g}$ (solid lines), as well as the one of $f_{esc,i}$ (dotted lines) is shown.

rates. This is due to the fact that in our case the ionisation rate is distributed among various sources located at different heights above the midplane.

In Fig. 4 the time evolution of the escape fraction is shown, for a Gaussian (lower curves) and a fractal (upper curves) density distribution. As a reference, we have chosen a run that produces, for both distributions and given the same set of stars (with $\dot{N}_\gamma = 2 \times 10^{50} \text{ s}^{-1}$), a comparable value of $f_{esc,g}$. The solid (dotted) lines indicate the evolution of $f_{esc,g}$ ($f_{esc,i}$). As in a GDD photons can escape only through ionised channels produced by the stars themselves, the photon escape is retarded and the evolution of f_{esc} is steeper compared to the case of a FDD. Initially, $f_{esc,i}$, which becomes constant after $\approx 10^6$ yr, is higher than $f_{esc,g}$. This is due to the fact that, when the first photons escape (at a time $t \sim 10^3$ [10⁵] yr for a FDD [GDD]), a large number of photons has already been emitted and this results in a very low value of $f_{esc,g}$. Then $f_{esc,g}$ increases, approaching $f_{esc,i}$.

In Figs. 5 and 6 illustrative slices extracted from the simulation box for the same run of Fig. 4, show the evolution of the ionised gas (black regions) produced by the sources in the given density field. The top six panels are for a GDD and show the ionised regions at a time $t = 0.1$ Myr from the source turn on, at different vertical distances from the midplane. The bottom six panels are the same for a FDD. As already pointed out above, although in the GDD the upper gas layers at this time are still neutral, some ionising photons have already escaped the FDD. In Fig. 6 the top (bottom) six panels refer to the GDD (FDD). Here we show the time evolution (columns, from left to right, refer to $t = 0.005, 0.5, 5$ Myr respectively) of slices at two heights above

the midplane. Again, the ionised regions are more extended in a fractal than in a Gaussian medium.

Although in this work we focus on the variation of f_{esc} with the different density distribution, it is interesting to check the values we obtain for the column density of the neutral gas. For runs A and B, we should be able to recover the observed Galactic HI column density ($N_{HI} = 5.2 \times 10^{20} \text{ cm}^{-2}$), i.e. about 30% of the total gas should be ionised (Sect. 2.1). For a GDD (run A) we obtain a final mean HI column density of $N_{HI} = 2.1 \times 10^{20} \text{ cm}^{-2}$, i.e. about 40% lower; for a FDD (run B), $N_{HI} = 4.1 \times 10^{20} \text{ cm}^{-2}$ is closer to the observed value. In both cases, however, some of the simulations have column density closer to the observed. Despite the larger escape fraction for a FDD, the resulting mean HI column density is larger for a fractal medium, where the highest density regions are more difficult to ionise and recombine faster. Also with an increased stellar surface density (runs C and D) the mean N_{HI} in a FDD remains as high as $\approx 2.7 \times 10^{20} \text{ cm}^{-2}$, while in a GDD it is $\approx 5.9 \times 10^{19} \text{ cm}^{-2}$, with values as low as $\approx 10^{17} \text{ cm}^{-2}$. The reduced ionisation fraction in the case of an inhomogeneous medium was also noted in the model for the diffused ionised medium of Miller & Cox (1993), which took into account the absorption of UV radiation by clouds with density larger than the surrounding medium in a statistical way.

In Fig. 7 the vertical distribution of the mean HI (solid lines) and HII (dotted lines) number densities is shown, for runs A and B with the above N_{HI} , in the case of a Gaussian (top panel) and fractal (bottom panel) density field at different times after the source turn on. For both distributions, the HI profile does not change until $t \approx 10^5$ yr, when the inner regions, where the stars reside, have an HII density of $n_{HII} \approx 0.1 \text{ cm}^{-3}$. The final HI density profile has a similar shape for both distributions, with a slightly lower value in the inner regions for a GDD case. The HII number density increases gradually in a FDD, while in a GDD, as previously mentioned, the ionisation of the upper gas layers is postponed until the stars have been able to produce an ionised channel for the escaping of photons. At the final stages, the HII distribution appears more extended than the HI one. This is consistent with observations of the Reynolds layer, which seems to have a vertical scale height of ≈ 1 kpc (Mezger 1978; Reynolds 1991a, 1991b). However, a proper modelling of the diffuse ionised gas should take into account the dynamical effects on gas, which would make the ionised gas to expand, as well as a larger vertical size for the simulation box.

In Fig. 8 we show the evolution of $f_{esc,g}$ as a function of the total ionisation rate for run B (filled circles) and E (stars), the only difference being the stellar distribution. The distribution of the escape fraction looks similar in the two cases and the obtained values are comparable; in fact, in run E the stars, following the Gaussian distribution of the gas, have a larger vertical extension, but, as they are located in denser regions, more photons are needed to ionise them and the two effects roughly balance.

Finally, we present in Fig. 9 the spectrum of the emerging ionising radiation, for five realizations of runs A and B, respectively. In both plots, the uppermost curve is the intrinsic spectrum of stars, i.e. a black body with $T=40000$ K. As already discussed, each simulation is characterised by the rate of emitted ionising photons, \dot{N}_γ . Since we are mainly

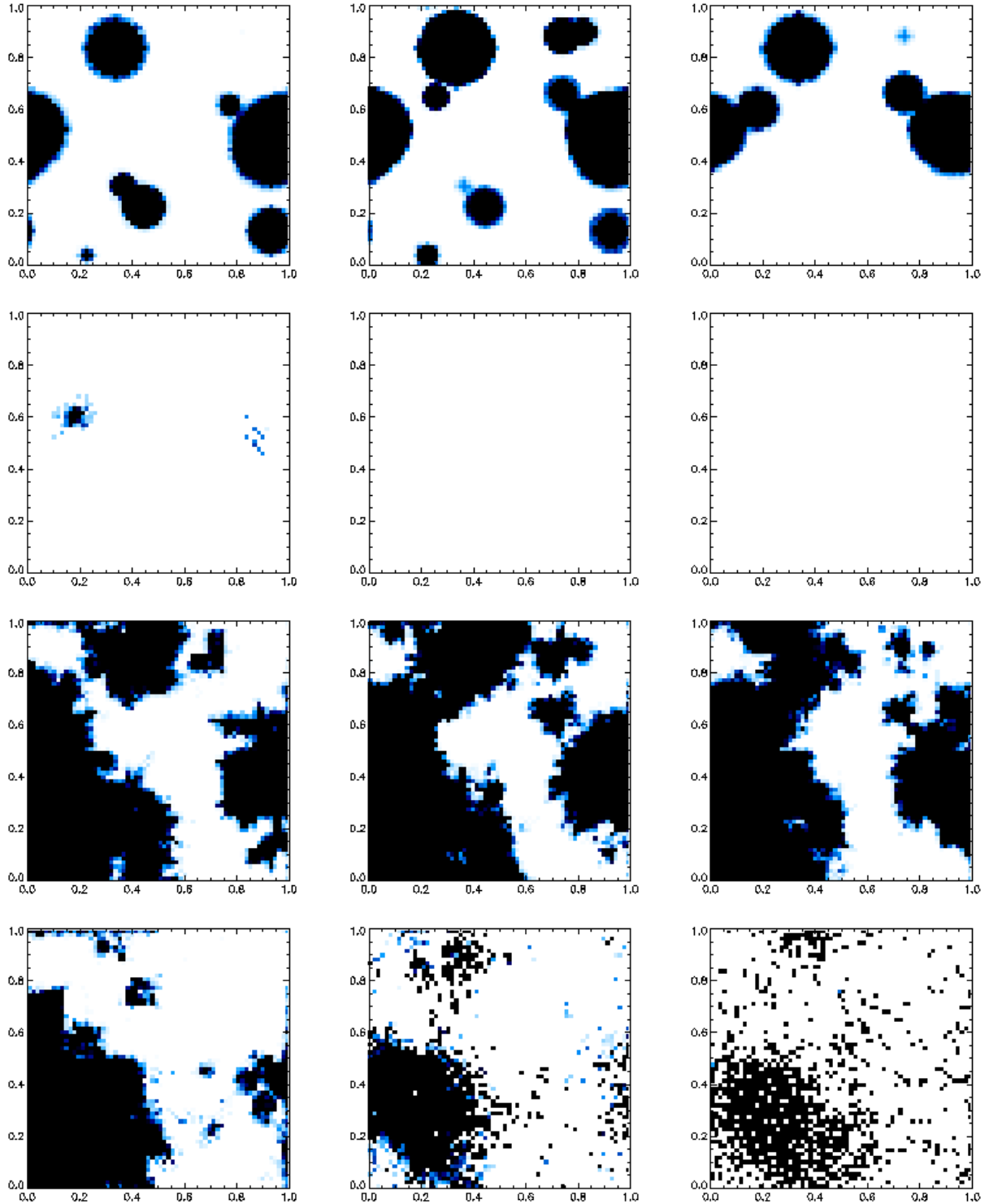


Figure 5. Evolution of ionisation field (black) produced by a given stellar distribution into a Gaussian (top six panels) and a fractal (bottom six panels) density field. The slices are taken at a time $t = 0.1$ Myr from the source turn on, at different vertical distances from the midplane (0, 10, 156, 312, 625, 940 pc, left to right).

interested in the shape of the spectrum, we normalise all simulations to the value $\dot{N}_\gamma = 2 \times 10^{50} \text{s}^{-1}$. As expected from the ν^{-3} frequency dependence of the HI photoionisation cross section, the emerging filtered spectrum is harder than the intrinsic one. For run A, the shape of the spec-

trum depends on the amount of escaping photons (*i.e.* on the escape fraction) in each realization: the lower and upper emerging spectra in the left panel of Fig. 9 being those for the lower and higher values of \dot{N}_γ . Different realizations of run B yield much more similar emerging spectra, this re-

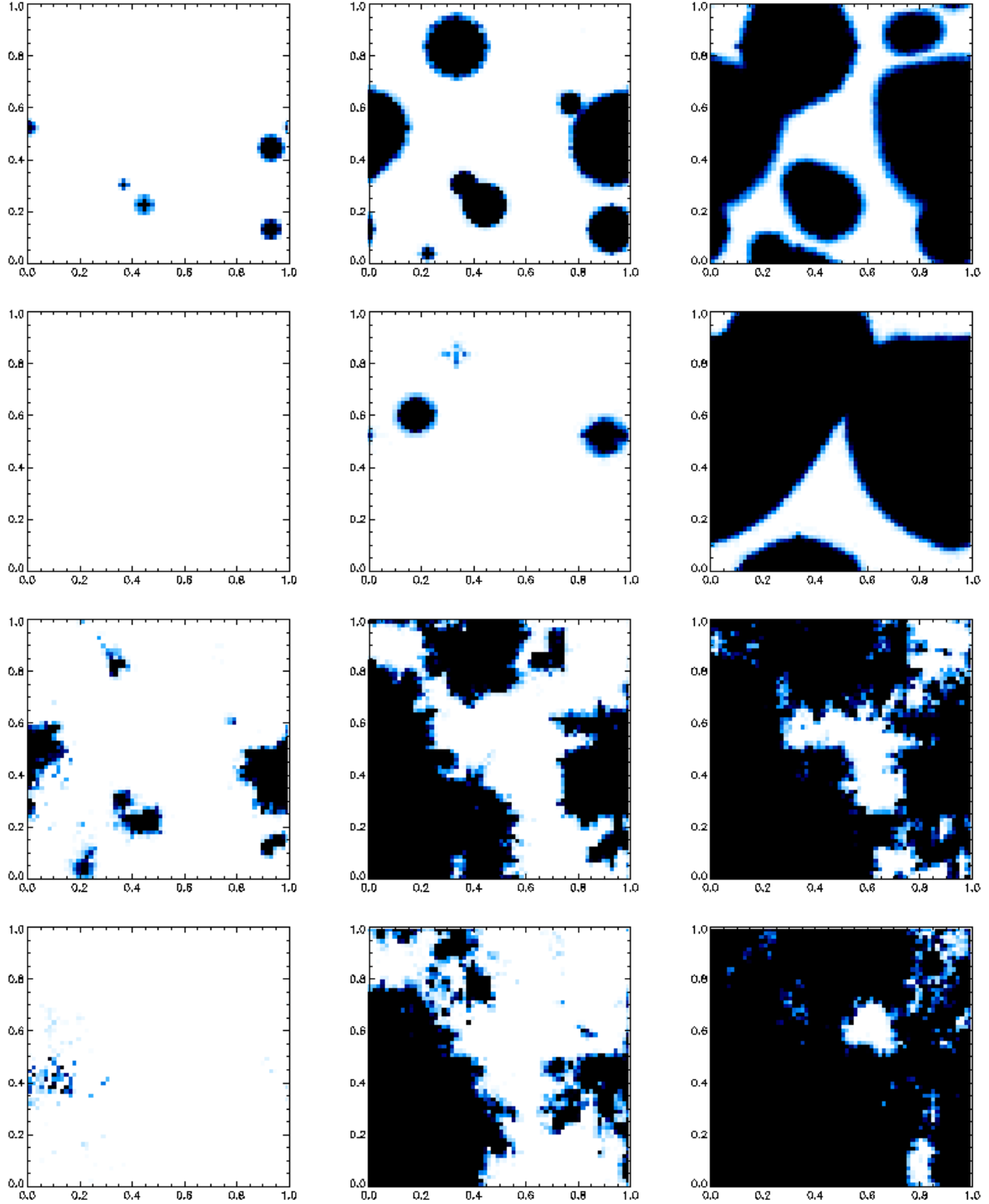


Figure 6. Evolution of ionisation field (black) produced by a given stellar distribution into a Gaussian (top six panels) and a fractal (bottom six panels) density field. The time evolution (columns, from left to right, refer to $t = 0.005, 0.5, 5$ Myr respectively) of slices at 0 (first row) and 265 pc (second row) above the midplane is shown.

flecting the nearly constant value of the escape fraction. As a reference, we plot in the right panel of Fig. 9 a black-body with $T=45000$ K. We remind that here we do not take into account the absorption of photons with $h\nu > 24.6$ eV by HeI, which may be the cause for the low HeI ionisation

observed in the diffuse ionised medium (Reynolds & Tufte 1995).

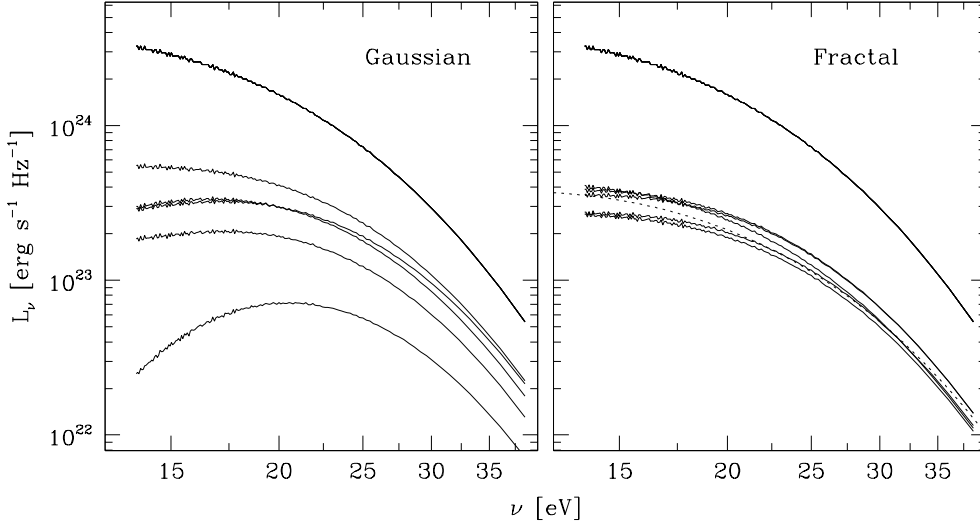


Figure 9. Spectrum of the emerging ionising radiation, for five realizations of run A (left panel) and run B (right panel). In both panels, the uppermost curve is the spectrum of the intrinsic ionising radiation (a blackbody with $T=40000$ K). For ease of presentation, all the spectra have been normalised to an intrinsic photon rate $\dot{N}_\gamma = 2 \times 10^{50} \text{ s}^{-1}$. The dotted curve in the right panel is a blackbody with $T=45000$ K.

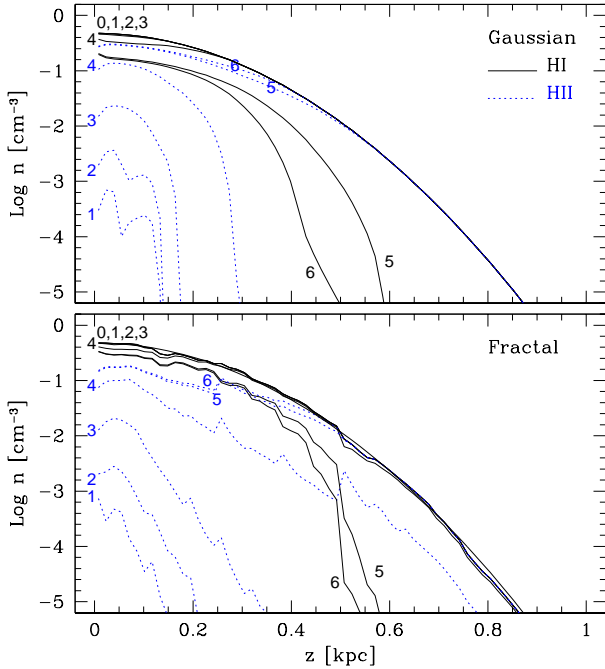


Figure 7. Vertical distribution of the mean HI (solid lines) and HII (dotted lines) number densities, in the case of a Gaussian (top panel) and fractal (bottom panel) density field. The numbers refer to different times from the source turn on: $i = 0 \dots 6$ refers, respectively, to $t = 0, 10^2, 10^3, 10^4, 10^5, 10^6$ and 10^7 yr.

5 SUMMARY AND CONCLUSIONS

We have studied the effects of gas density inhomogeneities on the escape of ionizing Lyman continuum photons from Milky Way-type galaxies via radiative transfer numerical simulations. To this aim a comparison between a smoothly stratified and an inhomogeneous, fractal distribution have

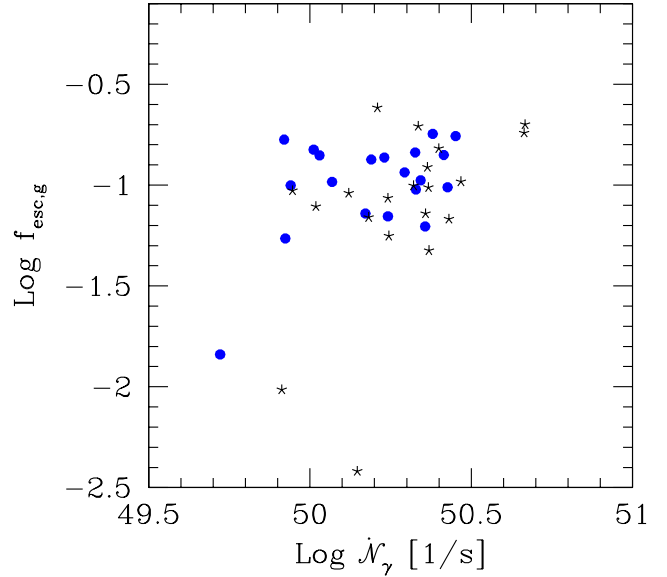


Figure 8. Evolution of the global escape fraction, $f_{esc,g}$, as a function of the total ionisation rate, \dot{N}_γ , for runs B (filled circles) and E (stars).

been made with realistic assumptions for the ionizing stellar sources based on available data in the solar neighborhood. The main results obtained can be summarized as follows.

(1) The global escape fraction, $f_{esc,g}$, in the case of a Gaussian Density Distribution (GDD) rapidly increases with increasing total ionization rate, \dot{N}_γ , and it flattens for high values of \dot{N}_γ ; for a Fractal Density Distribution (FDD) the dependence on \dot{N}_γ is milder.

(2) For $\dot{N}_\gamma \lesssim 2 \times 10^{50} \text{ s}^{-1}$ $f_{esc,g}$ is always higher for a

FDD, while for larger ionization rate a GDD becomes more transparent.

(3) For low stellar surface densities, Σ_* , there is a large scatter in the results, due to differences in the star positions and ionization rates. The scatter is reduced for larger Σ_* , as the star position affects less sensibly the value of f_{esc} , which instead depends more strongly on \dot{N}_γ .

(4) In a GDD the photon escape is retarded and the time evolution of the escape fraction is steeper compared to the FDD case.

(5) For a GDD we obtain a final mean HI column density of $N_{HI} = 2.1 \times 10^{20} \text{ cm}^{-2}$, lower than the observed one; for a FDD, $N_{HI} = 4.1 \times 10^{20} \text{ cm}^{-2}$ closely matches the experimental value. In all cases, the HII distribution appears to be more extended than the HI one.

(6) The value of the escape fraction is more sensitive to the gas density rather than the stellar distribution.

In order to draw a more general conclusion from the results summarized above, it is useful to translate the total ionization rate into a star formation rate for a given galaxy. To do so we use the results of the stellar population synthesis code Starburst99 (Leitherer *et al.* 1999). Assuming a continuous star formation mode, a Salpeter IMF with $M_{down} = 1M_\odot$ and $M_{up} = 100M_\odot$ and a metallicity equal to 1/20 of solar, we find that the expected ionization rate inside our simulated kpc^3 produced by the corresponding stellar population is $\dot{N}_\gamma = 4.5 \times 10^{50} (\dot{M}_*/M_\odot \text{yr}^{-1})$. From Fig. 3 we then note that for $\dot{M}_* \approx 2M_\odot \text{yr}^{-1}$ the escape fraction is already equal to roughly 0.6 (0.28) for the GDD (FDD) case.

Star formation rates of a few tens of solar masses are commonly derived from observations of LBGs (Pettini *et al.* 2001). This result may suggest a galaxy-dominated UV background. In fact, Bianchi, Cristiani & Kim (2001) have recently shown that estimates of the local and high- z metagalactic ionizing flux are consistent with a galaxy-dominated background if $f_{esc} \approx 10\%$. Hence it appears that these type of sources, as long as they could be modelled as relatively normal disk galaxies, can strongly influence the ionization history of the intergalactic medium and, possibly, the galaxy formation process.

In principle, then, photons can escape rather efficiently (particularly if their ISM is smooth) from high redshift galaxies, provided their vertical gas distribution is not too different from the Milky-Way type galaxies investigated here. Although galactic disk models based on simple semi-analytical prescriptions (Fall & Efstathiou 1980; Mo, Mao & White 1998; Weil, Eke & Efstathiou 1998; Ferrara, Pettini & Shchekinov 2000; Wood & Loeb 2000) predict that the disk column density should increase with redshift by a factor ≈ 10 between the present value and redshift 5, this estimate is still subject to several uncertainties. For example it is not clear how both the gas temperature (governing the disk scaleheight) and the fraction of baryons that are able to cool and settle in the disk (determining the mid-plane gas density) evolve with cosmic time. Even if the column density is larger, we do expect that the galactic ISM is smoother than the present day one, due to the short time interval available for the build up of a fully developed turbulent spectrum and hence a fractal gas distribution. This process might require several (say, 10) eddy turnover times, t_e , on the scale at which turbulence is injected by super-

bubbles, *i.e.* $\ell \approx 1 \text{ kpc}$ (Norman & Ferrara 1996). If the characteristic eddy velocity is $v_t \approx 1 \text{ km s}^{-1}$, this implies that $t_e \approx 10 \text{ Gyr}$ is much longer than the Hubble time at redshift 3. Hence, a final conclusion from models like the one presented here extended to encompass high redshift galaxies have to await additional data (both observational and from galaxy formation models) on the distribution and dynamical state of the gas in primordial galaxies.

ACKNOWLEDGMENTS

We would like to thank A. Lorenzani and M. Normandeau for help with the HI density distributions and the referee, K. Wood, for useful comments. This work was partially supported by the Research and Training Network "The Physics of the Intergalactic Medium" set up by the European Community under the contract HPRN-CT2000-00126 RG29185.

REFERENCES

- Benson, A. J., Nusser, A., Sugiyama, S. & Lacey, C. G. 2001, MNRAS, 320, 153
- Bianchi, S., Cristiani, S. & Kim, T.-S. 2001, A&A, 376, 1
- Bland-Hawthorn, J. & Maloney, P. R. 1999, ApJ, 510, 33
- Bland-Hawthorn, J. & Maloney, P. R. 2001, ApJ, 550, 231
- Bohlin, R. C., Savage, B. D. & Drake, J. F. 1978, ApJ, 224, 132
- Burton, W. B. & Hartmann, D. 1994, Ap&SS, 217, 189
- Ciardi, B., Ferrara, A., Governato, F. & Jenkins, A. 2000, MNRAS, 314, 611
- Ciardi, B., Ferrara, A., Marri, S. & Raimondo, G. 2001, MNRAS, 324, 381
- Dickey, J. M. & Lockman, F. J. L. 1990, ARA&A, 28, 215
- Dove, J. B. & Shull, J. M. 1994a, ApJ, 423, 196
- Dove, J. B. & Shull, J. M. 1994b, ApJ, 430, 222
- Dove, J. B., Shull, J. M. & Ferrara, A. 2000, ApJ, 531, 846
- Elmegreen, B. G. 1997, ApJ, 477, 196
- Elmegreen, B. G. 1999, ApJ, 527, 266
- Elmegreen, B. G. & Falgarone, E. 1996, ApJ, 471, 816
- Falgarone, E., Phillips, T. G. & Walker, C. K. 1991, ApJ, 378, 186
- Fall, S. M. N. & Efstathiou, G. 1980, MNRAS, 193, 189
- Ferrara, A., Pettini, M., & Shchekinov, Y. 2000, MNRAS, 319, 539
- Fitzpatrick, E. L. & Massa, D. 1988, ApJ, 328, 734
- Giallongo, E., Fontana, A. & Madau, P. 1997, MNRAS, 289, 629
- Garmany, C. D., Conti, P. S. & Chiosi, C. 1982, 263, 777
- Giroux, M. & Shull, J. M. 1997, AJ, 113, 1505
- Gnedin, N. Y. & Ostriker, J. P. 1998, ApJ, 486, 581
- Gnedin, N. Y. 2000, ApJ, 535, 530
- Haehnelt, M. G., Madau, P., Kudritzki, R. & Haardt, F. 2001, ApJL, 549, 151
- Heckman, T. M. *et al.* 2001, ApJ, 558, 56
- Hurwitz, M., Jelinsky, P. & Dixon, W. V. 1997, ApJ, 481, L31
- Kulkarni, S. R. & Fich, M. 1985, ApJ, 289, 792
- Leitherer, C., Ferguson, H. C., Heckman, T. M. & Lowenthal, J. D. 1995, ApJL, 454, 19
- Leitherer, C. *et al.* 1999, ApJS, 123, 3
- Maíz-Apellániz, J. 2001, AJ, 121, 2737
- Mezger, P. G. 1978, A&A, 70, 565
- Miller, W. W. & Cox, D. P. 1993, ApJ, 417, 579.
- Miralda-Escudé, J., Haehnelt, M. & Rees, M. R. 2000, ApJ, 530, 1
- Mo, H. J., Mao, S. & White, S. D. M. 1998, MNRAS, 295, 319
- Norman, C. A. & Ferrara, A. 1996, ApJ, 467, 280

- Pettini, M. *et al.* 2001, ApJ, 554, 981
Reynolds, R. J. 1985, ApJ, 294, 256
Reynolds, R. J. 1991a, ApJ, 372, L17
Reynolds, R. J. 1991b, in *The Interstellar Disk-Halo Connection in Galaxies*, ed. H. Bloemen, (Dordrecht: Kluwer), p. 67
Reynolds, R. J. 1993, *Massive Stars: Their Lives in the Interstellar Medium*, ASP Conference Series, eds. J.P. Cassinelli & E.B. Churchwell, vol. 35, p. 338
Reynolds, R. J. & Haffner, L. M. 2001, preprint (astro-ph/0010618)
Reynolds, R. J. & Tufte, S. L. 1995, ApJ, 439, L17.
Ricotti, M. & Shull, J. M. 2000, ApJ, 542, 548
Sanders, B. D., Kraushaar, W. L., Nousek, J. A. & Fried, P. M. 1977, ApJ, 217, L87
Schaerer, D. & de Koter, A. 1997, A&A, 322, 598
Sfeir, D. M., Lallement, R., Crifo, F. & Welch, B. Y. 1999, A&A, 346, 785
Snowden, S. L., Cox, D. P., McCammon, D. & Sanders, W. T. 1990, ApJ, 354, 211
Steidel, C. C., Pettini, M. & Adelberger, K. L. 2001 ApJ, 546, 665
Weil, M. L., Eke, V. R. & Efstathiou, G. 1998, MNRAS, 300, 773
Witt, A. N. *et al.* 1993, ApJ 410 714
Wood, K. & Loeb, A. 2000, ApJ, 545, 86